

Nonvolatile Electrical Switching and Write-Once Read-Many-Times Memory Effects in Functional Polyimides Containing Triphenylamine and 1,3,4-Oxadiazole Moieties

Kun-Li Wang,^{*,†} Yi-Liang Liu,[‡] Jian-Wei Lee,[†] Koon-Gee Neoh,[‡] and En-Tang Kang[‡]

[†]Department of Chemical Engineering & Biotechnology, National Taipei University of Technology, Taipei 10608, Taiwan, and [‡]Department of Chemical & Biomolecular Engineering, National University of Singapore, Kent Ridge, Singapore 119260

Received March 23, 2010; Revised Manuscript Received July 27, 2010

ABSTRACT: This work reports the synthesis and characterization of a series of functional aromatic polyimides (OXTA-PIs) containing triphenylamine and 1,3,4-oxadiazole moieties. All the polyimides exhibit high glass transition temperatures of 309–319 °C. A resistive switching device with the sandwich structure of indium–tin oxide/polymer/Al was fabricated using the soluble polyimide from 4,4'-hexafluoroisopropylidenediphthalic anhydride (OXTA-PIa). The device exhibits two conductivity states and can be switched from the initial low-conductivity (OFF) state to the high-conductivity (ON) state at the threshold voltages of 1.8 V under both positive and negative electrical sweeps, with an ON/OFF state current ratio in the order of 10⁵. The ON state of the device is nonvolatile and can withstand a constant voltage stress of –1 V for 6 h and 10⁸ pulse read cycles at –1 V under ambient conditions. Upon reversing the bias, the ON state cannot be reset to the initial OFF states. The nonvolatile and inerasable nature of the ON state, as well as the ability to write, read, and sustain the electrical states, fulfills the requirements of a write-once read-many-times (WORM) memory.

Introduction

Conventional microelectronics is based, to a large extent, on inorganic semiconductor integrated circuits. However, a number of physical and economic factors have threatened the continuous down scaling of silicon-based memory devices. These factors have motivated research into memory devices based on organic materials.^{1–3} Organic materials have certain attractive features over the inorganic materials, including flexibility, miniaturized dimensions, ease of processing, and the possibility for molecular design through chemical synthesis. In comparison to memory devices based on inorganic materials, polymer memories offer advantages including low-cost potential, good processability, good scalability, 3D stacking capability, large data storage capacity, and device flexibility.⁴ In contrast to memory devices based on inorganic materials, which store and retrieve data based on the amount of charge stored in the device, organic memory devices store data in another form, for instance, based on the electrical bistability in response to an applied electric field. A number of organic materials including conjugated molecules and polymers,^{5–7} dopants,⁸ and complex systems⁹ have been investigated for memory applications. Recently, polymer-based memory devices were reported to exhibit write-once read-many-times (WORM),^{10,11} flash (rewritable),^{12–14} static random access,^{15,16} and dynamic random access¹⁷ memory effects. The materials, devices, and mechanistic aspects of polymer electronic memories have been reviewed recently.¹⁸

Over the years, polyimides have been of interest in microelectronics because of their superior thermal and mechanical properties and low dielectric constants.¹⁹ Polyimides have also been investigated for applications in photovoltaics,^{20,21} light-emitting diodes,^{22,23} xerography,²⁴ and polymer memories.²⁵ In this work, a series of functional polyimides containing triphenylamine and

1,3,4-oxadiazole moieties have been synthesized and characterized. An electronic device based on the triphenylamine and 1,3,4-oxadiazole-containing polyimide derived from 4,4'-hexafluoroisopropylidenediphthalic anhydride (OXTA-PIa, structure shown in Schemes 1 and 2) was fabricated and studied for its electrical switching behavior under electrical sweeps. The device exhibits nonvolatile and irreversible memory effects and fulfills the requirements of a WORM memory.

Experimental Section

Materials. The materials hydroxylamine hydrochloride (from Alfa Aesar), ammonium chloride (from Showa), sodium azide (from Showa), 4-(diphenylamino)benzaldehyde (from Acros), pyridine (from Echo), 3,5-dinitrobenzoyl chloride (from Acros), hydrochloric acid (from Showa), hydrazine monohydrate (from Alfa Aesar), 10% palladium on activated carbon (Pd/C, from Merck), and tin(II) chloride anhydrous (from Sigma-Aldrich) were used as received. The solvents *N*-methyl-2-pyrrolidinone (NMP), *N,N*-dimethylacetamide (DMAc), dimethyl sulfoxide (DMSO), chloroform, and 1,4-dioxane were purchased from Tedia, and tetrahydrofuran (THF), *N,N*-dimethylformamide (DMF), methanol, ethanol, and acetic acid were purchased from Echo. NMP was purified by distillation under reduced pressure over calcium hydride and stored over 4 Å molecular sieves. Acetic anhydride was purchased from Acros and used as received. The aromatic tetracarboxylic dianhydrides, 4,4'-hexafluoroisopropylidenediphthalic anhydride (6FDA, from Chriskev), 4,4'-sulfonyldiphthalic anhydride (SDPA, from TCI), 3,3',4,4'-benzophenonetetracarboxylic dianhydride (BTDA, from Chriskev), 4,4'-oxidiphthalic anhydride (ODPA, from TCI), and pyromellitic dianhydride (PMDA, from Chriskev) were sublimated before use.

Instrumentation and Measurements. Fourier transform infrared (FT-IR) spectra were recorded on a Perkin-Elmer GX FT-IR spectrophotometer. NMR spectra were recorded using a Bruker DRX-500 NMR (¹H at 500.13 MHz and ¹³C at 125.76 MHz) spectrometer. Elemental analyses were performed on a

*To whom all correspondence should be addressed: Tel 886-2-77212171 ext 6411; e-mail klwang@ntut.edu.tw.

Perkin-Elmer 2400 instrument. The inherent viscosity of polyimides was measured using a Tamson viscometer. Thermogravimetric analyses (TGA) were carried out on a Shimadzu DTG-60/60H thermal analyzer under a nitrogen flowing rate of $50 \text{ cm}^3 \text{ min}^{-1}$ and a heating rate of $10 \text{ }^\circ\text{C min}^{-1}$. Differential scanning calorimetry (DSC) analyses were also performed on the Shimadzu DTG-60/60H thermal analyzer under a nitrogen flowing rate of $30 \text{ cm}^3 \text{ min}^{-1}$ and a heating rate of $10 \text{ }^\circ\text{C min}^{-1}$. Weight-average (M_w) and number-average (M_n) molecular weights were determined by gel permeation chromatography (GPC). Four Waters (Ultrastaygel) columns ($300 \times 7.7 \text{ mm}$, guarded and packed with $500, 10^3, 10^4$, and 10^5 \AA porous gels in series) were used for GPC analysis, using THF at a flow rate of 1 mL min^{-1} as the eluent. The eluents were monitored with a RI detector (JASCO Systems, RI-2031, Japan). Monodispersed polystyrene samples were used as the molecular weight standards. UV-vis absorption spectra were measured on a Cary UV 500 UV-vis-NIR spectrophotometer. Photoluminescence (PL) spectra were measured on a Perkin-Elmer LS 55 luminescence spectrophotometer. The thickness of the polymer film cast on the indium-tin oxide (ITO)-coated glass substrate was determined from the edge profile of the film, using the tapping mode, on a Veeco multimode atomic force microscope (AFM) equipped with a Nanosensors PPP-NCHR silicon tip. Cyclic voltammetry (CV) was performed on a CHI model 619A electrochemistry workstation with ITO as the working electrode

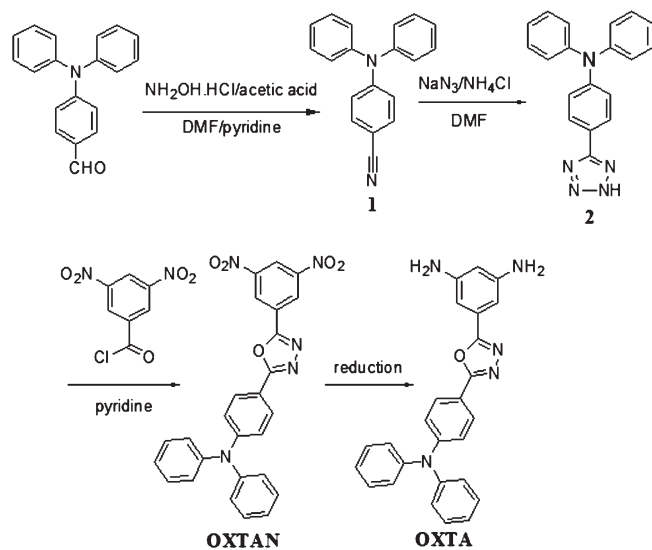
and a platinum wire as the auxiliary electrode at a scan rate of 50 mV s^{-1} against a Ag/Ag^+ reference electrode in a 0.1 M acetonitrile (CH_3CN) solution of tetrabutylammonium perchlorate (TBAP).

Device Fabrication and Characterization. The ITO-coated glass substrate was pre-cleaned sequentially with deionized water, acetone, and isopropanol in an ultrasonic bath for 15 min. A $100 \mu\text{L}$ DMAc solution of the functional polyimide (10 mg mL^{-1}) was spin-coated onto the ITO substrate at a spinning rate of 1200 rpm, followed by solvent removal in a vacuum oven at 10^{-5} Torr and $60 \text{ }^\circ\text{C}$ for 10 h. The thickness of the polyimide film was about 50 nm, as determined by the AFM edge profiling. Finally, Al top electrodes of about 400 nm in thickness was thermally deposited onto the polymer surface through a shadow mask at a pressure of about 10^{-7} Torr. Electrical property measurements were carried out on devices of $0.4 \times 0.4 \text{ mm}^2$, $0.2 \times 0.2 \text{ mm}^2$, and $0.15 \times 0.15 \text{ mm}^2$ in size, under ambient conditions, using an Agilent 4155C semiconductor parameter analyzer equipped with an Agilent 41501B pulse generator. The current density-voltage (J - V) data reported were based on device units of $0.4 \times 0.4 \text{ mm}^2$ in size, unless stated otherwise. ITO was maintained as the ground electrode during the electrical measurements.

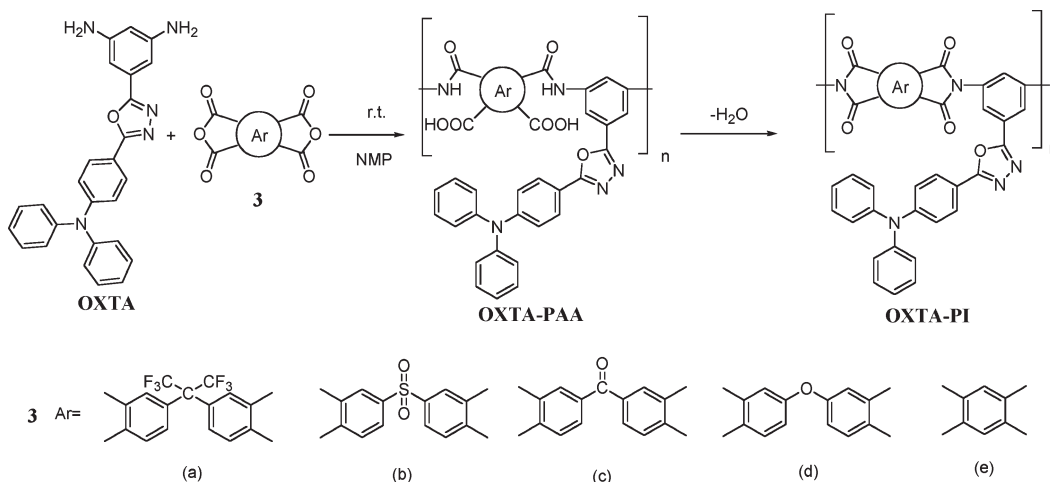
Synthesis of Monomers. *N*-(4-(5-(3,5-Dinitrophenyl)-1,3,4-oxadiazol-2-yl)phenyl)-*N*-phenylbenzenamine (OXTAN). Compounds **1** and **2** in Scheme 1 were prepared according to the methods reported in the literatures.^{26,27} A mixture of 2.0 g (6.38 mmol) of 4-tetrazolyltriphenylamine (**2**), 1.76 g (7.6 mmol) of 3,5-dinitrobenzoyl chloride, and 20 mL of pyridine was heated at $120 \text{ }^\circ\text{C}$ with stirring for 48 h in a 250 mL round-bottomed flask. After cooling, the mixture was poured into dichloromethane (100 mL), washed with water ($30 \text{ mL} \times 3$), and dried over anhydrous MgSO_4 . The solvent was removed under reduced pressure. The residue was recrystallized from chloroform to afford the pure product. The yield of the orange product (OXTAN) was 2.0 g (65%); mp $193 \text{ }^\circ\text{C}$. FT-IR (KBr, cm^{-1}): 1537, 1340 ($-\text{NO}_2$ stretch), 1592 ($-\text{C}=\text{N}-$). $^1\text{H NMR}$ (CDCl_3 , δ , ppm): 7.11 (d, $J = 8.9 \text{ Hz}$, 2H), 7.20 (m, $J = 7.5 \text{ Hz}$, 6H), 7.36 (t, $J = 7.8 \text{ Hz}$, 4H), 7.96 (d, $J = 8.9 \text{ Hz}$, 2H), 9.13 (t, $J = 2 \text{ Hz}$, 1H), 9.2 (d, $J = 1.9 \text{ Hz}$, 2H). Anal. Calcd for $\text{C}_{26}\text{H}_{17}\text{N}_5\text{O}_5$: C, 65.13%; H, 3.57%; N, 14.61%. Found: C, 65.19%; H, 3.64%; N, 14.80%.

5-(5-(4-(Diphenylamino)phenyl)-1,3,4-oxadiazol-2-yl)benzene-1,3-diamine (OXTA). A mixture of 1.0 g (2.08 mmol) of nitro compound (OXTAN), 0.3 g of 10% Pd/C, 4 mL of hydrazine monohydrate, and 40 mL of ethanol was refluxed with stirring for 2 h in a 250 mL three-necked flask. The mixture was then filtered to remove Pd/C, followed by solvent removed in a rotary evaporator to afford the pure product. The yield of

Scheme 1. Synthesis of the New Diamine Monomer OXTA



Scheme 2. Synthesis of Polyimides (OXTA-PIs) via a Two-Step Condensation and Chemical Imidization Reaction



the pale yellow product (OXTA) was 0.74 g (88%); mp 245 °C. FT-IR (KBr, cm^{-1}): 3446, 3380, 3323, 3213 ($-\text{NH}_2$ stretch), 1592 ($-\text{C}=\text{N}-$). ^1H NMR (DMSO- d_6 , δ , ppm): 5.10 (s, 4H, NH_2), 6.02 (d, $J = 1.71$ Hz, 1H), 6.52 (d, $J = 1.8$ Hz, 2H), 7.03 (d, $J = 8.8$ Hz, 2H), 7.17 (m, $J = 6.2$ Hz, 6H), 7.39 (t, $J = 7.8$ Hz, 4H), 7.87 (d, $J = 8.8$ Hz, 2H). ^{13}C NMR (DMSO- d_6 , δ , ppm): 102.46, 149.87, 100.79, 124.02, 164.51, 163.30, 115.58, 127.73, 120.47, 150.31, 146.09, 125.55, 129.88, 124.64. Anal. Calcd for $\text{C}_{26}\text{H}_{17}\text{N}_5\text{O}$: C, 74.44%; H, 5.05%; N, 16.70%. Found: C, 74.47%; H, 4.96%; N, 16.73%.

Synthesis of Polymers (Scheme 2). To a stirring solution of 0.2 g (0.477 mmol) of OXTA in 2.0 mL of NMP, 0.21 g (0.477 mmol) of 4,4'-hexafluoroisopropylidenediphthalic anhydride (**3a**) was gradually added. The mixture was stirred at ambient temperature for 4 h to form the poly(amic acid) (OXTA-PAA). Chemical imidization was carried out by addition of 1.0 mL of acetic anhydride and 0.5 mL of pyridine into the above-mentioned poly(amic acid) solution, followed by heating at 120 °C for 3 h. The polymer solution was poured slowly into 300 mL of methanol. The precipitate (OXTA-PIa) was removed by filtration, washed with hot methanol, and dried at 100 °C under reduced pressure. FT-IR (film, cm^{-1}): 1785 (asymmetrical $\text{C}=\text{O}$ stretch), 1730 (symmetrical $\text{C}=\text{O}$ stretch), and 1351 cm^{-1} ($\text{C}-\text{N}$ stretch). ^1H NMR (DMSO- d_6 , δ , ppm): 7.07–6.93 (d, 8H), 7.29 (s, 4H), 7.58 (s, 3H), 7.93–7.68 (m, 7H), 8.06–8.03 (t, 2H), 8.29–8.18 (d, 4H).

Other polyimides, OXTA-PIb, OXTA-PIc, OXTA-PId, and OXTA-PIe, in Scheme 2, were prepared by similar procedures from OXTA and the corresponding dianhydrides, SDPA (**3b**), BTDA (**3c**), ODPA (**3d**), and PMDA (**3e**).

Results and Discussion

Monomer Synthesis. The synthesis route of 5-(5-(4-(diphenylamino)phenyl)-1,3,4-oxadiazol-2-yl)benzenediamine monomer (OXTA) is shown in Scheme 1. 4-Tetrazolyltriphenylamine (**2**) reacts with 3,5-dinitrobenzoyl chloride to afford the dinitro compound (OXTAN). The FT-IR spectrum of OXTAN showed characteristic bands of nitro groups at 1340 and 1537 cm^{-1} . Reduction of OXTAN in ethanol with hydrazine monohydrate in the presence of a catalytic amount of Pd/C at the reflux temperature produced the new compound (OXTA). The FT-IR and NMR spectroscopic data confirmed the structure of OXTA. The characteristic absorptions of nitro groups at 1340 and 1537 cm^{-1} disappeared, and new absorptions at 3239 and 3348 cm^{-1} ($\text{N}-\text{H}$ stretching) appeared in the FT-IR spectrum. The NMR spectra with peak assignments, including ^1H NMR, ^{13}C NMR, and two-dimensional COSY and HMQC spectra, of OXTA are shown in Figure S1 (Supporting Information). When OXTAN was reduced to a diamine, a chemical shift at 5.10 ppm, characteristic of amino groups, appeared in the ^1H NMR spectrum. These results confirm that the compound (OXTA) synthesized herein is consistent with the proposed structure.

Synthesis of Polymers. The functional polyimides OXTA-PIa to OXTA-PIe in Scheme 2 were prepared via the conventional two-step method by reacting equimolar of the novel diamine (OXTA) with the respective aromatic dianhydrides (**3a–3e**) to form the poly(amic acids) at ambient temperature, followed by chemical cyclodehydration (Scheme 2). Chemical imidization of the poly(amic acids) with a dehydrating agent, such as a mixture of acetic anhydride and pyridine, was also effective in preparing the polyimides. The polymer structures were confirmed by FT-IR and NMR spectroscopies. All the polyimides exhibited characteristic absorption bands of the imide ring near 1785 (asymmetric $\text{C}=\text{O}$ stretch), 1730 (symmetric $\text{C}=\text{O}$ stretch), and 1351 cm^{-1} ($\text{C}-\text{N}$ stretch). The ^1H NMR spectrum of the polyimide, OXTA-PIa, is shown in the Supporting Information (Figure S2). Assign-

Table 1. Solubility of the OXTA-PI Functional Polyimides^a

polymer code	solubility ^b						
	NMP	DMAc	DMSO	DMF	THF	CHCl_3	1,4-dioxane
OXTA-PIa	++	++	++	++	++	++	++
OXTA-PIb	+	±	±	+	–	–	±
OXTA-PIc	±	±	±	±	±	±	–
OXTA-PId	±	–	–	–	–	–	–
OXTA-PIe	–	–	–	–	–	–	–

^a Abbreviations: NMP: *N*-methyl-2-pyrrolidinone; DMAc: *N,N*-dimethylacetamide; DMF: *N,N*-dimethylformamide; DMSO: dimethyl sulfoxide; THF: tetrahydrofuran. ^b Solubility: measure in the concentration of 1 mg mL^{-1} ; ++, soluble at room temperature; +, soluble on heating; ±, partially soluble on heating; –, insoluble on heating.

Table 2. Thermal Properties of the OXTA-PI Functional Polyimides

polymer code	T_g^a (°C)	T_d at 5% weight loss in N_2 (°C) ^b	T_d at 10% weight loss in N_2 (°C) ^b	char yield in N_2 (%) ^c
OXTA-PIa	317	442	476	27
OXTA-PIb	317	440	472	43
OXTA-PIc	319	428	464	35
OXTA-PId	309	431	463	12
OXTA-PIe	– ^d	440	471	29

^a Glass transition temperature (T_g) measured by DSC at a heating rate of 10 °C min^{-1} . ^b Decomposition temperature recorded on DTG at a heating rate of 10 °C min^{-1} . ^c Char yield (%) at 800 °C. ^d Not observed.

ments of each proton are also given in the spectrum, and the chemical shifts are consistent with the proposed polymer structure. The polyimide OXTA-PIa obtained by chemical imidization had an inherent viscosity of 0.25 dL g^{-1} in DMAc. The number-average molecular weight (M_n) and weight-average molecular weight (M_w) of OXTA-PIa were 2.7×10^4 and 5.5×10^4 , respectively, giving rise to a polydispersity index ($\text{PDI} = M_w/M_n$) of 2.03. The molecular weights of other polyimides could not be measured by GPC due to their poor solubility.

Polymer Properties. The solubility of the synthesized polyimides in common organic solvents is shown in Table 1. The solubility of polyimides is dependent on their chain packing efficiency and intermolecular interactions, which in turn are influenced by the rigidity, symmetry, and regularity of the molecular backbone.²⁸ Among these polyimides, those derived from more rigid dianhydrides, OXTA-PIb, OXTA-PIc, OXTA-PId, and OXTA-PIe, had poor solubilities. The polyimide OXTA-PIa exhibits the best solubility in a variety of solvents, such as NMP, DMAc, DMF, DMSO, THF, chloroform, and 1,4-dioxane, at room temperature. Many studies have reported that the presence of hexafluoroisopropylidene groups in 6FDA introduces steric hindrance that prohibits close packing of the chains and increases the affinity of the chains for polar solvents.²⁹

Thermal Properties. The thermal properties of the polyimides were evaluated by differential scanning calorimetry (DSC) and thermogravimetric analysis (TGA), and the results are summarized in Table 2. The glass transition temperatures (T_g) of the polyimides were found to range from 309 to 319 °C. The polyimide OXTA-PId obtained from ODPA (**3d**) showed the lowest T_g (309 °C) because of the presence of a flexible ether linkage between the phthalimide units. OXTA-PIa exhibits a much higher glass transition temperature than that of the previously reported P(BPPO)-PI¹⁵ (structure shown in Figure 1a) with a similar molecular structure (317 °C for OXTA-PIa vs 250 °C for P(BPPO)-PI), probably due to the more rigid molecular chain in OXTA-PIa in the absence of the flexible phenoxy

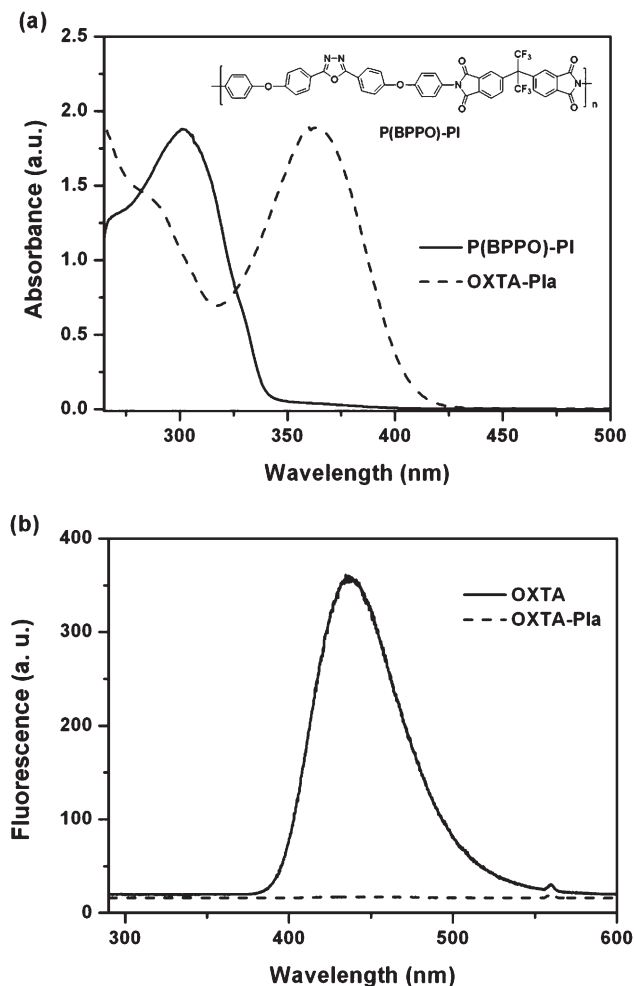


Figure 1. (a) Normalized UV-vis absorption spectrum of OXTA-PIa in chloroform with that of P(BPPO)-PI as the reference. (b) Emission spectrum of OXTA-PIa in chloroform with that of the diamine monomer, OXTA, as the reference.

group.³⁰ The thermal stability of the polyimides was evaluated by TGA under a nitrogen atmosphere at a heating rate of $10\text{ }^{\circ}\text{C min}^{-1}$. The temperatures for 10% weight loss of the polyimides in nitrogen range from 463 to 476 $^{\circ}\text{C}$. The char yields of the polyimides at 800 $^{\circ}\text{C}$ in nitrogen range from 12 to 43 wt %.

Optical Properties. The optical properties of the polyimide OXTA-PIa were investigated by UV-vis absorption and photoluminescence (PL) spectroscopies in chloroform. Figure 1a shows the UV-vis absorption spectra of OXTA-PIa in chloroform, with P(BPPO)-PI¹⁵ as the reference. The concentration of P(BPPO)-PI was about $5 \times 10^{-7}\text{ mol L}^{-1}$. The concentration of OXTA-PIa was adjusted to make the number of its repeat units comparable to those of P(BPPO)-PI. The absorption spectra are normalized to the maximum absorption peak of P(BPPO)-PI for ease of comparison. As shown in Figure 1a, the P(BPPO)-PI solution exhibits a maximum absorption peak at 301 nm, which is attributed to the $\pi \rightarrow \pi^*$ transition of the π -electronic system delocalized along the 2,5-bis(4-phenoxyphenyl)-1,3,4-oxadiazole (BPPO) moieties.³¹ In comparison to P(BPPO)-PI, an additional triphenylamine group is incorporated into the OXTA-PIa molecule, resulting in significant enhancement of the intramolecular charge transfer (CT) and thus inducing a CT absorption band at 364 nm.³¹ The absorption edge of OXTA-PIa extends to about 407 nm, from which the band

gap energy (E_g) of OXTA-PIa is determined to be 3.05 eV. The PL spectra of OXTA-PIa ($6.7 \times 10^{-7}\text{ mol L}^{-1}$) and the diamine monomer OXTA in chloroform are shown in Figure 1b. The concentration of OXTA was adjusted to be comparable to that of the repeat units of OXTA-PIa. The emission spectra were obtained with an excitation wavelength of 280 nm. As shown in Figure 1b, the OXTA monomer exhibits an intense emission peak at 436 nm, which is red-shifted by about 100 nm in comparison to the emission of 2,5-diphenyl-1,3,4-oxadiazole.³³ This large red shift arises probably from the intense CT between the triphenylamine and oxadiazole groups in OXTA. The fluorescent quantum yield (Φ_F) of the monomer (OXTA) in chloroform was estimated by comparison with the PL of standard 9,10-diphenylanthracene. The fluorescent quantum yield of OXTA was 23.6%. The fluorescence of OXTA-PIa, however, was significantly quenched, indicating a considerable decay of the excited singlet state of the OXTA moieties in the polymer due to CT between the OXTA and phthalimide moieties.³⁴

Electrochemical Properties. The electrochemical properties of the polyimide OXTA-PIa were investigated by cyclic voltammetry conducted in a 0.1 M dry acetonitrile solution of TBAP under a nitrogen atmosphere for the film deposited on a platinum disk electrode. The polymer exhibited an oxidation peak at 0.60 V, with the onset located at 0.49 V. The highest occupied molecular orbital (HOMO) and lowest unoccupied molecular orbital (LUMO) energy levels can be calculated from the onset oxidation potential [$E_{\text{Ox}}(\text{onset})$] and the band gap of the copolymer based on the reference energy level of ferrocene (4.8 eV below the vacuum level, which is defined as zero)

$$\begin{aligned} \text{HOMO} &= -[(E_{\text{Ox}}(\text{onset}) - E_{\text{Foc}}) + 4.8] \quad (\text{eV}) \\ \text{LUMO} &= \text{HOMO} + E_g \quad (\text{eV}) \end{aligned} \quad (1)$$

According to these formulas, the HOMO and LUMO energy levels for OXTA-PIa are calculated to be -5.18 and -2.13 eV, respectively.

Electrical Switching Behavior of the Functional Polyimide. Electrical switching and memory effects of OXTA-PIa were tested by examining the current-voltage (J - V) characteristics of an ITO/OXTA-PIa/Al sandwich device, as shown in Figure 2a. Initially, the as-fabricated device was in the low-conductivity (OFF) state. The current density remained low during the first negative sweep (with Al as the cathode and ITO as the anode) from 0 to -3 V until the switching threshold voltage of -1.8 V was reached. At this voltage, the current density increased abruptly from 10^{-7} to 10^{-2} A cm^{-2} , indicating the device transition from the initial OFF state to the high-conductivity (ON) state. This electrical transition is equivalent to the “writing” process in a digital memory cell. The ON/OFF current ratio was in the order of 10^5 at -1 V. The device exhibited good stability in the ON state during the subsequent negative and positive sweeps, and it did not return to the OFF state even after turning off the power (the second sweep) or upon applying a reverse sweep (the third sweep). The nonvolatile and irerasable nature of the ON state suggests that the OXTA-PIa device exhibits WORM type memory.

In addition to the electrical switching effect, other parameters, such as stability and read cycles, are of equal importance to the performance of a memory device. All of these parameters were evaluated under ambient conditions. Figure 2b shows the effect of operation time on the memory device. Under a constant stress of -1 V, no obvious degradation in current density was observed for both the ON

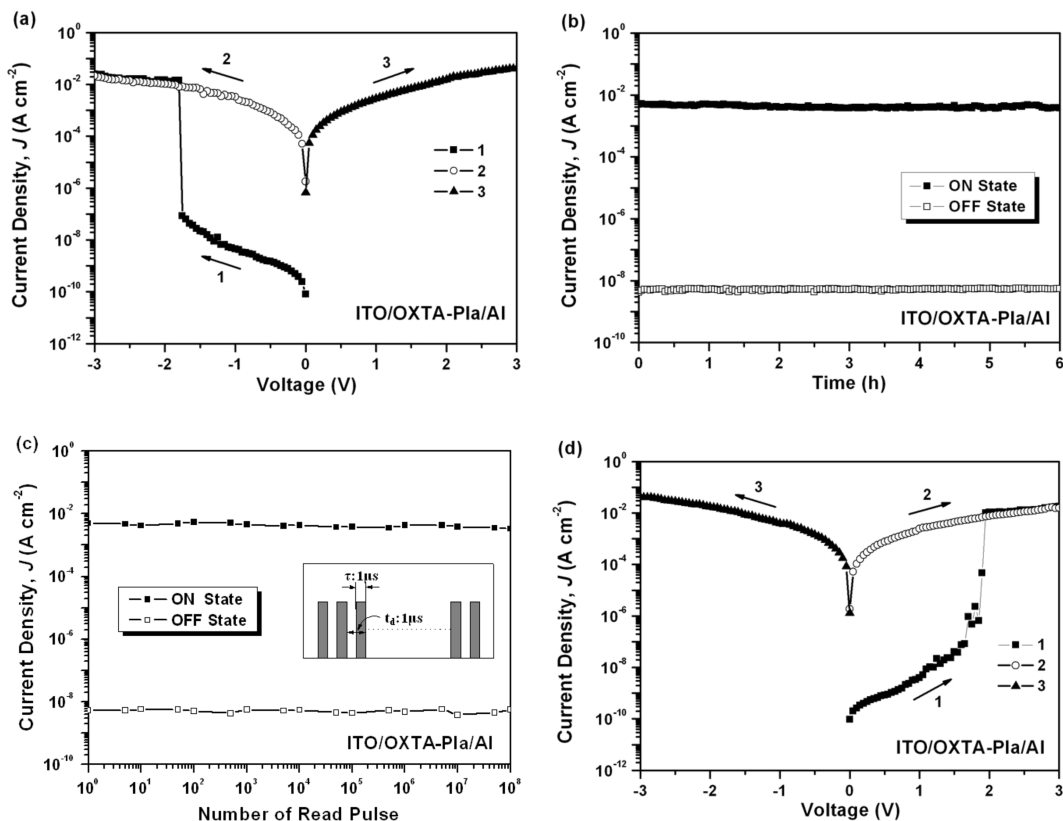


Figure 2. (a) Current density–voltage (J – V) characteristics of OXTA-PIa in a $0.4 \times 0.4 \text{ mm}^2$ ITO/polymer/Al device with an initial negative electrical sweep. The sequence and direction of each sweep are indicated by the respective number and arrow. (b) Effect of operation time on the ON and OFF states of the memory devices under a constant stress of -1 V. (c) Effect of read pulse of -1 V on the ON and OFF states of the memory device. (d) Current density–voltage (J – V) characteristics of OXTA-PIa in a $0.4 \times 0.4 \text{ mm}^2$ ITO/polymer/Al device with an initial positive electrical sweep.

and OFF states of the present device. The ON and OFF states are also stable up to 1×10^8 read pulses of -1 V, as shown in Figure 2c. These results indicate that these memory devices exhibit good stability and performance. Devices with different active areas of $0.4 \times 0.4 \text{ mm}^2$, $0.2 \times 0.2 \text{ mm}^2$, and $0.15 \times 0.15 \text{ mm}^2$ showed almost the same J – V characteristics, indicating that the current density was independent of the device area. The area-independent current density, good reproducibility of the J – V characteristics, and stability of the memory effects rule out the possibility of filament conduction³⁵ or polymer degradation effects in the present device.

The memory device based on OXTA-PIa can also exhibit electrical switching if the initial electrical sweep is positive. As shown in Figure 2d, the device was initially swept positively from 0 to 3 V. An abrupt increase in the current density was observed at the switching threshold voltage of 1.8 V, which is comparable in magnitude to the negative switching threshold voltage of -1.8 V. The results indicate that the OXTA-PIa device can be switched bidirectionally, with comparable positive and negative switching threshold voltages.

Forrest et al. reported WORM memory devices based on poly(ethylene dioxythiophene) (PEDOT):poly(styrenesulfonic acid) (PSS) films.^{10,11} The switching of the PEDOT:PSS film from a high to a low conductivity state has been explained by a simple undoping process. Thermal effects arising from Joule heating play a significant role in destabilizing the PEDOT:PSS complex formed by CT interaction.¹¹ To further understand the switching phenomenon in the present OXTA-PIa, attempts were made, in vain, to heat a device in the ON state to above T_g . At temperature above T_g , the polymer softened and the device failed due to the difference in expansion

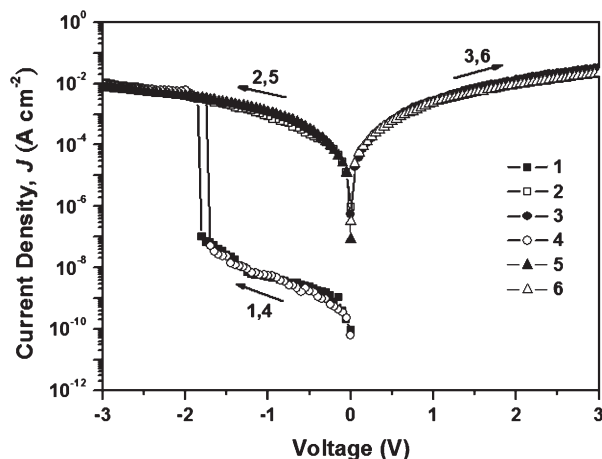


Figure 3. J – V characteristics of an ITO/OXTA-PIa/Al device. The sequence and direction of each sweep are indicated by the respective number and arrow. The 4th–6th sweeps were conducted sequentially after heating the device at 150°C for 10 min under vacuum.

coefficients between the polymer and electrodes. To avoid device degradation, a device in the ON state was heated at 150°C for 10 min. The switching behavior of the device after heating is shown in Figure 3. The device in the initial OFF state was switched to ON state at -1.8 V and retained in the ON state as described above (first to third sweeps). Interestingly, after being heated at 150°C for 10 min and then cooled to room temperature, the device in the ON state was found to return to its OFF state (the fourth sweep). The device could be switched again to the ON state at the threshold voltage of

−1.7 V and remained in the ON state during the subsequent negative and positive sweeps. It could not be returned to the OFF state even after turning off the power (the fifth sweep) or upon applying a reverse sweep (the sixth sweep). The results indicate that the turn-on phenomenon probably do not originate from chemical reactions.

The phthalimide group is a strong electron acceptor³⁶ while the triphenylamine group is a strong electron donor.³⁷ Thus, under an electric field, electrons can transfer from the triphenylamine donor to the phthalimide acceptor, via the oxadiazole mediator group, to give rise to an abrupt increase in the current density and the electrical switching from the initial OFF state to the ON state.

Conclusions

This study reports the synthesis of a series of aromatic polyimides with triphenylamine and oxadiazole units in the pendant groups. All the polyimides exhibit good thermal stability. The polyimide from 4,4'-hexafluoroisopropylidenedipthalic anhydride (OXTA-PIa) also exhibits good solubility and thus processability. Bistable electrical switching devices based on the OXTA-PIa thin films exhibit nonvolatile and irreversible WORM memory effects with symmetric bidirectional switching threshold voltages of ± 1.8 V. The electric field-induced charge transfer from the triphenylamine donor to the phthalimide acceptor may account for the observed electrical switching and memory effects.

Acknowledgment. The authors thank the National Science Council (NSC) of Taiwan for the financial support (NSC98-2221-E-027-002) and Taipei Medical University and National Taiwan Normal University for the NMR measurements.

Supporting Information Available: Additional data, ¹H NMR, ¹³C NMR, and two-dimensional COSY and HMQC spectra of the novel diamine OXTA (Figure S1), ¹H NMR spectrum of OXTA-PIa (Figure S2), and GPC elution curve of the soluble polyimide OXTA-PIa (Figure S3). This material is available free of charge via the Internet at <http://pubs.acs.org>.

References and Notes

- (1) Das, B. C.; Pal, A. J. *ACS Nano* **2008**, *2*, 1930–1938.
- (2) Yonekuta, Y.; Susuki, K.; Oyaizu, K.; Honda, K.; Nishide, H. *J. Am. Chem. Soc.* **2007**, *129*, 14128–14129.
- (3) Cai, L.; Feng, M.; Guo, H. M.; Ji, W.; Du, S. X.; Chi, L. F.; Fuchs, H.; Gao, H. J. *J. Phys. Chem. C* **2008**, *112*, 17038–17041.
- (4) Stikeman, A. *Technol. Rev.* **2002**, *105*, 31–31.
- (5) Pradhan, B.; Das, S. *Chem. Mater.* **2008**, *20*, 1209–1211.
- (6) Yook, K. S.; Lee, J. Y.; Kim, S. H.; Jang, J. *Appl. Phys. Lett.* **2008**, *92*, 223305.
- (7) Kim, T. W.; Oh, S. H.; Choi, H.; Wang, G.; Hwang, H.; Kim, D. Y.; Lee, T. *Appl. Phys. Lett.* **2008**, *92*, 253308.
- (8) Lai, Q. X.; Zhu, Z. H.; Chen, Y.; Patil, S.; Wudl, F. *Appl. Phys. Lett.* **2006**, *88*, 133515.
- (9) Weitz, R. T.; Walter, A.; Engl, R.; Sezi, R.; Dehm, C. *Nano Lett.* **2006**, *6*, 2810–2813.
- (10) Möller, S.; Perlov, C.; Jackson, W.; Taussig, C.; Forrest, S. R. *Nature* **2003**, *426*, 166–169.
- (11) Smith, S.; Forrest, S. R. *Appl. Phys. Lett.* **2004**, *84*, 5019–5021.
- (12) Ling, Q. D.; Chang, F. C.; Sang, Y.; Zhu, C. X.; Liaw, D. J.; Chan, D. S. H.; Kang, E. T.; Neoh, K. G. *J. Am. Chem. Soc.* **2006**, *128*, 8732–8733.
- (13) Wang, K. L.; Tseng, T. Y.; Tsai, H. L.; Wu, S. C. *J. Polym. Sci., Part A: Polym. Chem.* **2008**, *46*, 6861–6871.
- (14) You, N. H.; Chueh, C. C.; Liu, C. L.; Ueda, M.; Chen, W. C. *Macromolecules* **2009**, *42*, 4456–4463.
- (15) Liu, Y. L.; Wang, K. L.; Huang, G. S.; Zhu, C. X.; Tok, E. S.; Neoh, K. G.; Kang, E. T. *Chem. Mater.* **2009**, *21*, 3391–3399.
- (16) Kuorosawa, T.; Chueh, C. C.; Liu, C. L.; Higashihara, T.; Ueda, M.; Chen, W. C. *Macromolecules* **2010**, *43*, 1236–1244.
- (17) Liu, Y. L.; Ling, Q. D.; Kang, E. T.; Neoh, K. G.; Liaw, D. J.; Wang, K. L.; Liou, W. T.; Zhu, C. X.; Chan, D. S. H. *J. Appl. Phys.* **2009**, *105*, 044501.
- (18) Ling, Q. D.; Liaw, D. J.; Zhu, C. X.; Chan, D. S. H.; Kang, E. T.; Neoh, K. G. *Prog. Polym. Sci.* **2008**, *33*, 917–978.
- (19) Meador, M. A. *Annu. Rev. Mater. Sci.* **1998**, *28*, 599–630.
- (20) Kotov, B. V.; Romyantsev, B. M.; Berendyaev, V. I.; Lunina, E. V.; Bespalov, B. P.; Frankevich, E. L.; Triebel, M. M. *Synth. Met.* **2001**, *121*, 1553–1554.
- (21) Lozano, A. E.; Abajo, J.; Campa, J. G.; Guillén, C.; Herrero, J.; Gutiérrez, M. T. *J. Appl. Polym. Sci.* **2007**, *103*, 3491–3497.
- (22) Kim, Y.; Lee, J. G.; Han, K.; Hwang, H. K.; Choi, D. K.; Jung, Y. Y.; Keum, J. H.; Kim, S.; Park, S. S.; Im, W. B. *Thin Solid Films* **2000**, *363*, 263–267.
- (23) Shin, J. H.; Park, J. W.; Lee, W. K.; Jo, N. J.; Cho, W. J.; Ha, C. S. *Synth. Met.* **2003**, *137*, 1017–1018.
- (24) Wang, Z. Y.; Qi, Y.; Cao, J. P.; Sacripante, G. C.; Sundararajan, P. R.; Duff, J. D. *Macromolecules* **1998**, *31*, 2075–2079.
- (25) Ling, Q. D.; Liaw, D. J.; Teo, E. Y. H.; Zhu, C. X.; Chan, D. S. H.; Kang, E. T.; Neoh, K. G. *Polymer* **2007**, *48*, 5182–5201.
- (26) Bing, Y. J.; Leung, L. M.; Menglian, G. *Tetrahedron. Lett.* **2004**, *45*, 6361–6363.
- (27) Tamoto, N.; Adachi, C.; Nagai, K. *Chem. Mater.* **1997**, *9*, 1077–1085.
- (28) Wang, K. L.; Liou, W. T.; Liaw, D. J.; Huang, S. T. *Polymer* **2008**, *49*, 1538–1546.
- (29) Liaw, D. J.; Wang, K. L. *J. Polym. Sci., Part A: Polym. Chem.* **1996**, *34*, 1209–1217.
- (30) Jin, S. H.; Kim, M. Y.; Kim, J. Y.; Lee, K.; Gal, Y. S. *J. Am. Chem. Soc.* **2004**, *126*, 2474–2480.
- (31) Wolarz, E.; Chrzumnicka, E.; Fischer, T.; Stumpe, J. *Dyes Pigm.* **2007**, *75*, 753–760.
- (32) Tao, Y. T.; Wang, Q.; Shang, Y.; Yang, C. L.; Ao, L.; Qin, J. H.; Ma, D. G.; Shuai, Z. G. *Chem. Commun.* **2009**, 77–79.
- (33) Franco, O.; Orgzall, I.; Regenstein, W.; Schulz, B. *J. Phys.: Condens. Matter* **2006**, *18*, 1459–1472.
- (34) Lukas, A. S.; Zhao, Y. Y.; Miller, S. E.; Wasielewski, M. R. *J. Phys. Chem. B* **2002**, *106*, 1299–1306.
- (35) Henish, H. K.; Smith, W. R. *Appl. Phys. Lett.* **1974**, *24*, 589–591.
- (36) Freilich, S. C. *Macromolecules* **1987**, *20*, 973–978.
- (37) Redecker, M.; Bradley, D. D. C.; Inbasekaran, M.; Wu, W. W.; Woo, E. P. *Adv. Mater.* **1999**, *11*, 241–246.